Probing the Symmetry Energy with the Spectral Pion Ratio

J. Estee,[1,2,*] W. G. Lynch,[1,2,†] C. Y. Tsang,[1,2] J. Barney,[1,2] G. Jhang,[1] M. B. Tsang,[1,2,‡] R. Wang,[1] M. Kaneko,[3,4] J. W. Lee,[5] T. Isobe,[3,§] M. Kurata-Nishimura,[3] T. Murakami,[3,4,‖] D. S. Ahn,[3] L. Atar,[6,7] T. Aumann,[6,7] H. Baba,[3] K. Boretzky,[7] J. Brzychczyk,[8] G. Cerizza,[1] N. Chiga,[3] N. Fukuda,[3] I. Gasparic,[9,3,6] B. Hong,[5] A. Horvat,[6,7] K. Ieki,[10] N. Inabe,[3] Y. J. Kim,[11] T. Kobayashi,[12] Y. Kondo,[13] P. Lasko,[14] H. S. Lee,[11] Y. Leifels,[7] J. Łukasik,[14] J. Manfredi,[1,2] A. B. McIntosh,[15] P. Morfouace,[1] T. Nakamura,[13] N. Nakatsuka,[3,4] S. Nishimura,[3] H. Otsu,[3] P. Pawłowski,[14] K. Pelczar,[8] D. Rossi,[6] H. Sakurai,[3] C. Santamaria,[1] H. Sato,[3] H. Scheit,[6] R. Shane,[1] Y. Shimizu,[3] H. Simon,[7] A. Snoch,[16] A. Sochocka,[8] T. Sumikama,[3] H. Suzuki,[3] D. Suzuki,[3] H. Takeda,[3] S. Tangwancharoen,[1] H. Toernqvist,[6,7] Y. Togano,[10] Z. G. Xiao,[17] S. J. Yennello,[15,18] and Y. Zhang[17]

(SπRIT Collaboration)

M. D. Cozma[1,19,¶]

[1]*National Superconducting Cyclotron Laboratory, Michigan State University, East Lansing, Michigan 48824, USA*
[2]*Department of Physics, Michigan State University, East Lansing, Michigan 48824, USA*
[3]*RIKEN Nishina Center, Hirosawa 2-1, Wako, Saitama 351-0198, Japan*
[4]*Department of Physics, Kyoto University, Kita-shirakawa, Kyoto 606-8502, Japan*
[5]*Department of Physics, Korea University, Seoul 02841, Republic of Korea*
[6]*Institut für Kernphysik, Technische Universität Darmstadt, D-64289 Darmstadt, Germany*
[7]*GSI Helmholtzzentrum für Schwerionenforschung, Planckstrasse 1, 64291 Darmstadt, Germany*
[8]*Faculty of Physics, Astronomy, and Applied Computer Science, Jagiellonian University, Kraków, Poland*
[9]*Division of Experimental Physics, Rudjer Boskovic Institute, Zagreb, Croatia*
[10]*Department of Physics, Rikkyo University, Nishi-Ikebukuro 3-34-1, Tokyo 171-8501, Japan*
[11]*Rare Isotope Science Project, Institute for Basic Science, Daejeon 34047, Republic of Korea*
[12]*Department of Physics, Tohoku University, Sendai 980-8578, Japan*
[13]*Department of Physics, Tokyo Institute of Technology, Tokyo 152-8551, Japan*
[14]*Institute of Nuclear Physics PAN, ul. Radzikowskiego 152, 31-342 Kraków, Poland*
[15]*Cyclotron Institute, Texas A&M University, College Station, Texas 77843, USA*
[16]*Nikhef National Institute for Subatomic Physics, Amsterdam, Netherlands*
[17]*Department of Physics, Tsinghua University, Beijing 100084, People's Republic of China*
[18]*Department of Chemistry, Texas A&M University, College Station, Texas 77843, USA*
[19]*IFIN-HH, Reactorului 30, 077125 Măgurele-Bucharest, Romania*

(Received 26 January 2021; revised 8 March 2021; accepted 22 March 2021; published 19 April 2021)

Many neutron star properties, such as the proton fraction, reflect the symmetry energy contributions to the equation of state that dominate when neutron and proton densities differ strongly. To constrain these contributions at suprasaturation densities, we measure the spectra of charged pions produced by colliding rare isotope tin (Sn) beams with isotopically enriched Sn targets. Using ratios of the charged pion spectra measured at high transverse momenta, we deduce the slope of the symmetry energy to be $42 < L < 117$ MeV. This value is slightly lower but consistent with the L values deduced from a recent measurement of the neutron skin thickness of ^{208}Pb.

DOI: 10.1103/PhysRevLett.126.162701

Recent gravitational wave measurements of the neutron star merger event GW170817 provide information about the deformability of neutron stars (NSs) [1,2]. Analyses of the gravitational wave signal reveal that this deformability mainly reflects the nuclear equation of state (EOS) at densities of about twice the saturation density of nuclear matter, $\rho_0 \approx 2.6 \times 10^{14}$ g/cm^3 or 0.16 /fm^3. While the GW170817 observations provide key insights into NSs and their mergers, they do not reveal how the NS EOS depends on the abundances of its constituent neutrons, protons, Δ resonances, and pions [3–12]. To understand what is the prevailing form of matter in the NS outer core, such microscopic information is essential.

Microscopic information about the EOS has only been extracted from laboratory experiments. Measurements of nucleus-nucleus collisions have constrained the EOS for

symmetric matter comprised of equal proton ρ_p and neutron ρ_n densities for total densities $\rho = \rho_n + \rho_p$ of $\rho_0 \leq \rho \leq 4.5\rho_0$ [13–15]. The main challenge for asymmetric systems is to understand the symmetry energy, which describes how the EOS depends upon isovector potentials that have the opposite sign for neutrons as for protons and depend linearly on the difference between neutron and proton densities $(\rho_n - \rho_p)$ or, equivalently, on the isospin asymmetry $\delta = (\rho_n - \rho_p)/\rho$ [3,7,9,16–18].

The symmetry energy has been constrained at subsaturation densities using a variety of nuclear structure and reaction observables [16,17,19]. To probe higher densities, one must study central collisions between two complex nuclei. At incident energies of about 300 AMeV and above, nuclear matter can be compressed to densities approaching $2\rho_0$ [20]. The isovector mean field potentials cause the flow of neutrons emitted from this dense region to differ from the flow of protons; this difference provides an observable that can constrain the symmetry energy [18,21].

In these dense regions, nucleon-nucleon inelastic collisions produce Δ baryons that decay to nucleons by emitting pions. From the Δ production and decay cross sections, one expects the ratio $M(\pi^-)/M(\pi^+)$ of the multiplicity (M) of negatively and positively charged pions per collision to be proportional to $(\rho_n/\rho_p)^2$ [18,22]. Because the ratio (ρ_n/ρ_p) strongly reflects the isovector mean field potentials within this dense region, both the total pion multiplicity yield ratio $M(\pi^-)/M(\pi^+)$ [18,23] and the dependence of the pion ratio on pion momentum [23–25] reflect the density dependence of the symmetry energy. Existing studies of $M(\pi^-)/M(\pi^+)$ [26,27] with stable nuclear beams have not provided a consistent constraint on the symmetry energy at suprasaturation densities $\rho > \rho_0$. This may result from different assumptions for the Δ and pion potentials that cause the calculated low energy pion spectra, the $M(\pi^-)/M(\pi^+)$ ratios and the symmetry energy constraints to differ [28].

Powerful new radioactive isotope facilities are being built to investigate how nuclei and the nuclear EOS depend on $\delta = (\rho_n - \rho_p)/\rho$ [16,18,29]. Here we present results from the first experiment at these new facilities to probe the symmetry energy at high density with radioactive beams. In this experiment, beams of ^{132}Sn, ^{124}Sn, ^{112}Sn, and ^{108}Sn projectiles at 270 A MeV incident energy bombarded isotopically enriched (> 95%) ^{124}Sn and ^{112}Sn targets of 608 and 561 mg/cm^2 areal density at the Radioactive Ion Beam Factory in Japan. Light charged particles, including π^- and π^+ mesons, were detected in a new device, the SπRIT time projection chamber (TPC), placed inside the superconducting analyzer for multiparticles from radioisotope beams (SAMURAI) spectrometer [30].

Previous publications describe the design and performance of the SπRIT TPC [31–33], its trigger systems [34], electronics readout system [35], and analysis software [36,37]. To measure minimum ionizing pions as well as isotopically resolved H, He, and Li isotopes, we expanded the typical dynamic range of the TPC electronics by a factor of 5 [38]. To seamlessly measure pions over the essential range of scattering angles, we placed the target at the entrance of the TPC and corrected for space charge effects from the beam traversing the TPC [39].

Charged particles were identified by their electronic stopping powers dE/dx and magnetic rigidities [36]. To optimize momentum resolution, pion data are measured at azimuthal angles $-40° < \phi < 25° \cup 160° < \phi < 210°$, where the pion momenta are mainly perpendicular to the magnetic field. Clean pion identification was achieved. We utilize ϕ independence and interpolate the pion spectra to other azimuthal angles where the momentum resolution would be inferior. We fit the dE/dx distributions for each momentum bin to determine the particle yield and the background contribution.

We focus on the most central collisions with the highest charged particle multiplicities corresponding to impact parameters of $b < 3$ fm [33]. Electrons and positrons from the Dalitz decay of π^0 are the largest contributions to the pion background and have been subtracted as detailed in Ref. [40]. These background contributions are insignificant.

The TPC pion acceptance in the current experiment allows energy of pions to be accurately measured down to 0 MeV in the c.m. of the total system. We focus on pions measured to polar angles of $\theta_{\text{c.m.}} < 90°$ with respect to the beam where pion acceptance is complete. This angular cut is also applied to the theoretical calculations discussed later. We calculate the efficiency by embedding Monte Carlo pion tracks into real events and determining the fraction of these tracks that are accurately reconstructed. We used a calibration beam composed of hydrogen isotopes at well-known momenta to check the momentum determination of the TPC. The momentum values obtained by using the TPC design geometry and SAMURAI dipole magnetic field agreed to within 1% of the known values [41]. The estimated systematic uncertainties are 4% for the individual pion spectra and 2% for the single and double ratios of charged pion spectra. These uncertainties are incorporated into the discussion below.

The total π^- and π^+ multiplicities and their ratios for central ($b \approx 3$ fm) ^{132}Sn + ^{124}Sn, ^{112}Sn + ^{124}Sn, and ^{108}Sn + ^{112}Sn collisions are published in Ref. [42]. Comparisons of the total pion ratios predicted by seven different theoretical calculations exhibit differences among them that exceed their sensitivity to the symmetry energy. Different assumptions regarding the mean field potentials for Δ baryons and pions can strongly influence the production of low energy pions and thus the total charged pion multiplicities and their ratios [28]. To reduce this sensitivity, we focus on pion spectra at higher momenta where sensitivity to the isospin dependence of the nucleonic mean fields dominates [28]. Using the pion spectral

ratios at high transverse momenta, we obtain a correlated constraint at suprasaturation densities on the symmetry energy and the momentum dependence of the isovector nucleonic mean field potentials.

For our investigations, we use the dcQMD semiclassical quantum molecular dynamics (QMD) model of Ref. [28]. This model has provided constraints on the symmetry energy from neutron and proton elliptic flow measurements [21] and from pion production [27,43]. It also provides reasonable predictions of the pion multiplicities and ratios for the current experiment [42]. A unique aspect of the dcQMD model is the implementation of the conservation of total energy for the system, which is not simply satisfied at the two-body level due to the momentum and isospin asymmetry dependence of interactions. This involves modifying the collision term to allow for energy transfer between scattering particles and the rest of the system, leading to shifts of particle production thresholds [27,44,45]. With this correction, consistent constraints for the symmetry energy density dependence were obtained from pion production and elliptic flow [27]. Further details of this model can be found in Refs. [21,27,28,43].

At beam energies of 270 A MeV, high energy pions are primarily produced by exciting Δ (1232) baryons via two-nucleon $N+N \to N+\Delta$ inelastic scattering processes. These Δ's may scatter elastically or inelastically via $N+\Delta \to N+\Delta'$ or decay via $\Delta \to N+\pi$ producing pions. Pions, in turn, can be absorbed via $\pi+N \to \Delta$. Details of the Δ resonance production parametrization and its modification in nuclear medium can be found in Refs. [46,47]. The present calculations require realistic binding energies per nucleon, charge radii and neutron skins for projectile and target nuclei, and a good quantitative description of the experimental stopping, directed flow, and elliptic flow observables [48,49]. These prior analyses are consistent with the isoscalar effective mass $m^*/m = 0.7$, compressibility modulus $K_0 = 245$ MeV [28], and in-medium elastic nucleon-nucleon cross sections [50] used here.

The Gaussian wave functions for nucleons and pions in dcQMD have widths that reflect the experimental ratio of pion-to-proton charge radii [43]. Pions move under the influence of the Coulomb interaction and S and P wave pion optical potentials calculated with the "Batty-1" parameters of Refs. [43,51]. We find that the usual ansatz of setting the Δ potential in nuclear matter equal to that of nucleons leads to incorrect π^- and π^+ production thresholds and total multiplicities [28,42]. Therefore, we adjust the potential depths at saturation density and effective masses in the isoscalar and isovector channels [28] of the Δ to reproduce experimental total pion multiplicities and mean kinetic energies.

In dcQMD, the nuclear EOS is defined in terms of the energy per nucleon and is given by [52]

$$\frac{E}{N}(\rho,\delta) = \mathrm{KE}(\rho,\delta) + A_u\frac{\rho(1-\delta^2)}{4\rho_0} + A_l\frac{\rho(1+\delta^2)}{4\rho_0} + \frac{B}{\sigma+1}\frac{\rho^\sigma}{\rho_0^\sigma}(1-x\delta^2) + \frac{D}{3}\frac{\rho^2}{\rho_0^2}(1-y\delta^2) + \frac{1}{\rho\rho_0}\sum_{\tau,\tau'}C_{\tau\tau'}\int\int d^3\vec{p}\,d^3\vec{p}\,'\frac{f_\tau(\vec{r},\vec{p})f_{\tau'}(\vec{r},\vec{p}\,')}{1+(\vec{p}-\vec{p}\,')^2/\Lambda^2}. \quad (1)$$

Here, $\mathrm{KE}(\rho,\delta)$ is the kinetic energy, followed by four local potential energy terms that depend on density ρ and asymmetry δ. The final nonlocal term models Pauli exchange terms and the finite range of nucleon-nucleon interactions. Parameter D controls the compressibility $K_0 = 245$ MeV and skewness $Q_0 = -350$ MeV of symmetric matter, and x and y control slope L and curvature K_{sym} parameters of the symmetry energy $S(\rho)$. We correlate L and K_{sym} via $K_{\mathrm{sym}} = -488 + 6.728 \times L$ (MeV) and also set $S(\rho = 0.1\ /\mathrm{fm}^3) = 25.5$ MeV, consistent with nuclear mass and radius measurements [53,54].

The left and right panels of Fig. 1 show the c.m. transverse momentum spectra dM/dp_T at $\theta_{\mathrm{c.m.}} < 90°$ for the very neutron rich $^{132}\mathrm{Sn} + {}^{124}\mathrm{Sn}$ and the nearly symmetric $^{108}\mathrm{Sn} + {}^{112}\mathrm{Sn}$ systems, respectively. The difference in the p_T values for the maxima of the π^- and π^+ spectra reflects the influence of the Coulomb interaction. The calculations with $L = 80$ MeV, shown in the figure have been fitted to the total multiplicities by optimizing the Δ

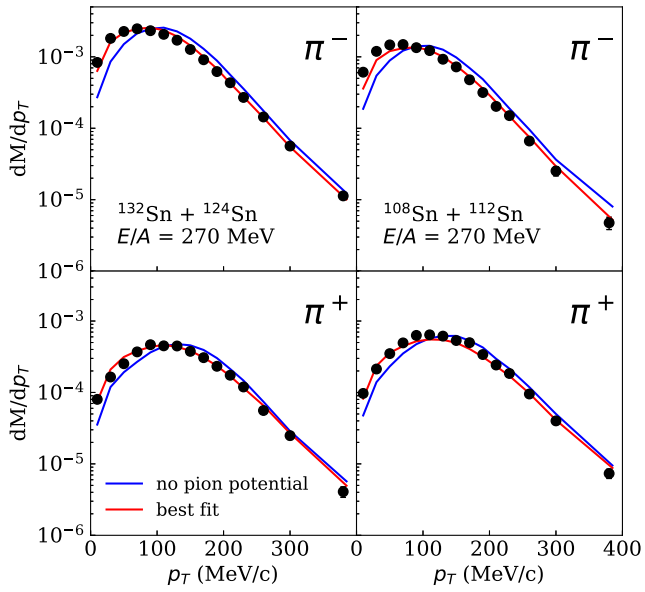

FIG. 1. Measured and calculated pion spectra. The red lines are the calculated pion spectra after adjusting the Δ potential to reproduce the pion multiplicities. The blue lines differ from the red lines in that the pion optical potential has been removed. The nucleon potentials in these simulations correspond to $L = 80$ MeV and $\Delta m^*_{np} = 0$.

potentials and effective masses. Here, the scaled difference between neutron and proton effective masses, $\Delta m^*_{np}/\delta = [m^*_n - m^*_p]/(m\delta)$ is set to zero. The red curves show the resulting calculations, including pion optical potentials, while the blue curves show calculations where pion potentials are removed. Simulations without the pion optical potential result in a significant underprediction of the pion spectra at low p_T and that extends over a larger range of momenta in the case of the π^+ spectra in both reactions. However, the shapes of the spectra at higher transverse momentum $p_T > 200$ MeV/c are largely unchanged by the choice of Δ and pion optical potentials, and remain sensitive to the nucleonic mean field potentials and to the symmetry energy [28]. Such sensitivities to the details in pion and Δ potentials for the low energy pions could account for the differences in transport code predictions for the total pion yields reported in Ref. [42].

Next, we focus on the isovector mean field potentials that contribute to the symmetry energy and are opposite in sign for neutrons vs protons and π^- vs π^+. We highlight these isovector potentials by constructing the single ratio $\mathrm{SR}(\pi^-/\pi^+) = [dM(\pi^-)/dp_T]/[dM(\pi^+)/dp_T]$. In Fig. 2, $\mathrm{SR}(\pi^-/\pi^+)_{132+124}$ for the neutron rich $^{132}\mathrm{Sn} + ^{124}\mathrm{Sn}$ system is shown in the top panel and $\mathrm{SR}(\pi^-/\pi^+)_{108+112}$ for the nearly symmetric $^{108}\mathrm{Sn} + ^{112}\mathrm{Sn}$ systems in the bottom panel. The steep rise in the single ratios at low p_T originates from the opposite Coulomb forces experienced by π^- and π^+.

We construct the pion single spectral ratios using dcQMD with 12 sets of calculations with values for L of (15, 60, 106, and 151 MeV) and $\Delta m^*_{np}/\delta$ of (−0.33, 0, and 0.33). For clarity, we show only four calculations with $(L, \Delta m^*_{np}/\delta) = (60, -0.33)$, (60, 0.33), (151, −0.33), and (151, 0.33) represented by blue solid, blue dashed, red solid, and red dashed curves, respectively. All calculations underpredict the data at $p_T < 50$ MeV/c and overpredict the data at $p_T \approx 150$ MeV/c for both systems. As expected, the neutron rich system of $^{132}\mathrm{Sn} + ^{124}\mathrm{Sn}$ displays much more sensitivity at high p_T to the slope of the symmetry energy L than does the nearly symmetric $^{108}\mathrm{Sn} + ^{112}\mathrm{Sn}$ system. The disagreement with data observed at low p_T for both systems suggests some inaccuracy in the theory that does not depend strongly on the asymmetry δ. Such effects could originate from inaccuracies in the treatment of Coulomb interactions or of the pion optical potentials above saturation density, for example. Nonresonant pion emission or absorption, neglected in the current calculations, could also contribute to the incorrect shape of the single spectral ratios at low p_T in Fig. 2 and its influence should be investigated. These effects should be much less important above 200 MeV/c, where the trends of the data and the calculations become more comparable.

Interpolating the dcQMD calculations, we fit the single ratios at $p_T > 200$ MeV/c and extract correlated

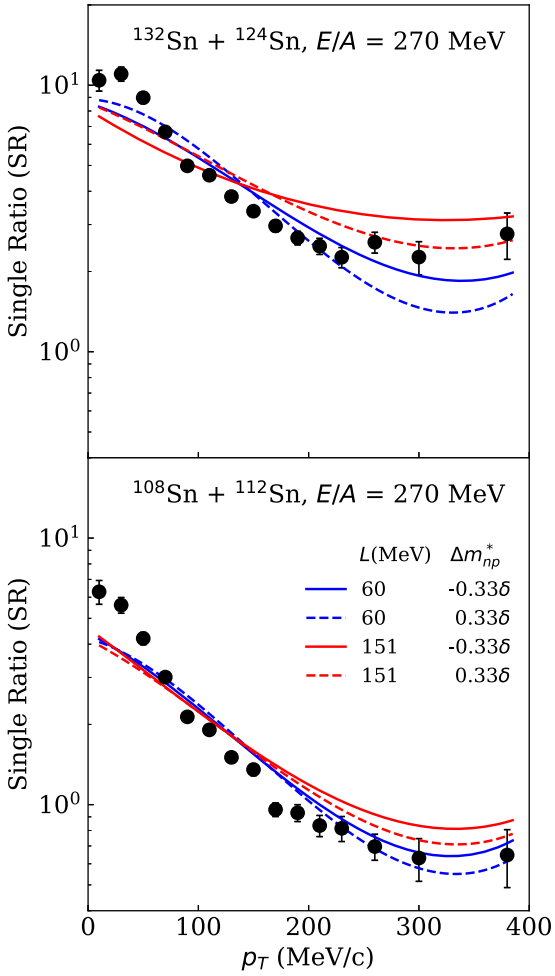

FIG. 2. Single pion spectral ratios for $^{132}\mathrm{Sn} + ^{124}\mathrm{Sn}$ (top) and $^{108}\mathrm{Sn} + ^{112}4\mathrm{Sn}$ (bottom) reactions. The curves are dcQMD predictions from different L and Δm^*_{np} values listed in the bottom panel.

constraints on L and $\Delta m^*_{np}/\delta$ shown in Fig. 3. The correlated nature of this constraint means that larger values for Δm^*_{np} would imply larger values for L. Absent any constraint on Δm^*_{np}, the best fit value is $L = 79.9 \pm 37.6$ MeV with $S_0 = 35.3 \pm 2.8$ MeV. The largest contribution to the total uncertainty is the statistical uncertainty. This value is consistent with constraints extracted from proton and neutron elliptic flows in Ref. [21] using the same transport model.

Since both reactions have the same total charge, approximately the same isoscalar fields, and differ principally by their asymmetry δ, the double ratio $\mathrm{DR}(\pi^-/\pi^+) = \mathrm{SR}(\pi^-/\pi^+)_{132+124}/\mathrm{SR}(\pi^-/\pi^+)_{108+112}$ should primarily reflect the isovector mean fields that determine the symmetry energy. Experimentally, the double ratio cancels out most of the systematic errors but the statistical errors propagate. The current uncertainties in the double ratios shown in Fig. 4 are large and thus offer less precise constraints than single ratios. Nonetheless, the data are

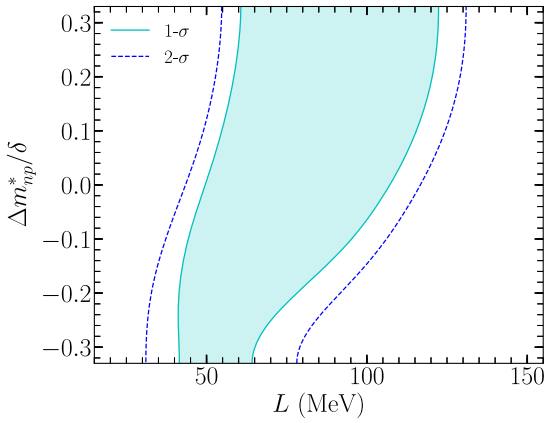

FIG. 3. Correlation contours between L and $\Delta m^*_{np}/\delta$ extracted from the single pion spectral ratio of the neutron rich $^{132}\mathrm{Sn} + ^{124}\mathrm{Sn}$ and near symmetric $^{108}\mathrm{Sn} + ^{112}\mathrm{Sn}$ reactions. The green shaded region lies within the 68% confidence level for data with $p_T > 200$ MeV/c. The dotted blue lines denote contours corresponding to the 95% confidence level.

statistically consistent with the predictions indicated by the shaded area allowed by the 1 σ range of the L values (49–105 MeV) assuming the most probable value of $\Delta m^*_{np}/\delta = 0$.

Additional measurements would reduce the uncertainties of this constraint. These include pion measurements at higher and lower incident energies to constrain nonresonant pion emission and the interactions of Δ baryons with nuclear matter. Precise measurements of the ratios of neutron and proton energy spectra should constrain Δm^*_{np} more accurately, removing an important contribution to the present uncertainty. Complementary measurements of proton and neutron elliptic flow are also desirable.

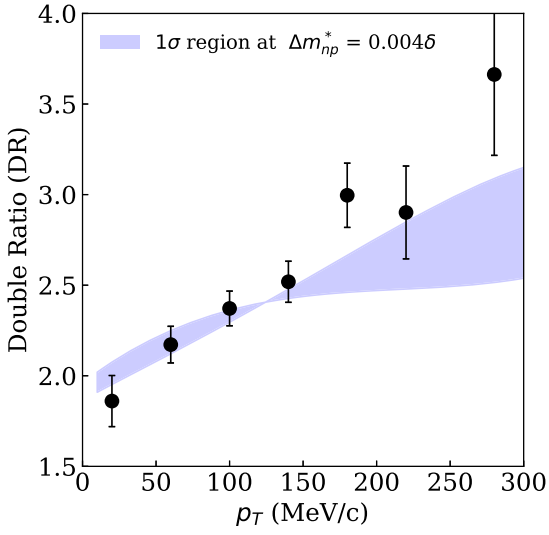

FIG. 4. Transverse momentum spectra of the double pion ratio. The shaded region covers dcQMD predictions within 1 σ of the most probable values of L and Δm^*_{np} values.

Finally, ongoing efforts in transport theory by the Transport Model Evaluation Project Collaboration (e.g., Ref. [55]) would allow a more comprehensive exploration of the equation of state of dense neutron rich matter via heavy ion collisions.

In conclusion, we present precise spectra of charged pions produced in intermediate energy collisions involving rare isotope Sn beams on isotopic Sn targets and use them to constrain the symmetry energy at suprasaturation densities. To avoid complications resulting from poorly constrained Δ baryon potentials and nonresonant pion emission that are currently difficult to model, we focus our analyses on energetic pions with $p_T > 200$ MeV/c and obtain symmetry energy constraints of $42 < L < 117$ and $32.5 < S_0 < 38.1$ MeV. The present results suggest a representative symmetry pressure of $P_{\mathrm{sym}} = 12 \pm 10$ Mev/fm^3 at $\rho/\rho_0 = 1.5$. These L values are smaller than the values $L = 106 \pm 37$ and $S_0 = 38.3 \pm 4.7$ MeV [56] extracted from a new measurement of the neutron skin thickness of ^{208}Pb [57], but close to the values $70 < L < 101$ and $33.5 < S_0 < 36.4$ MeV [58] extracted from charge exchange and elastic scattering reactions. We note that both the PREXII and charge exchange results are extrapolated from subsaturation density, while the pion results are extrapolated from suprasaturation density. These L values are larger than the L values [59,60] influenced by NS deformability [1,2] and radius [61,62] measurements.

The authors would like to thank Professor Hermann Wolter, Professor Che-Ming Ko, and Professor Pawel Danielewicz and the TMEP Collaboration for many fruitful discussions. This work was supported by the U.S. Department of Energy under Awards No. DE-SC0021235, No. DE-NA0003908, No. DE-FG02-93ER40773, No. DE-FG02-93ER40773, No. DE-SC0019209, No. DE-SC0015266, No. DE-AC02-05CH11231, U.S. National Science Foundation Grant No. PHY-1565546, the Robert A. Welch Foundation (A-1266 and A-1358), the Japanese MEXT, Japan KAKENHI (Grant-in-Aid for Scientific Research on Innovative Areas) Grant No. 24105004, JSPS KAKENHI Grants No. JP16H02179 and No. JP18H05404, the National Research Foundation of Korea under Grants No. 2016K1A3A7A09005578, No. 2018R1A5A1025563, No. 2013M7A1A1075764, the Polish National Science Center (NCN) under Contracts No. UMO-2013/09/B/ST2/04064, No. UMO-2013/-10/M/ST2/00624, the National Natural Science Foundation of China under Grant No. 11375094 and the Tsinghua University Initiative Scientific Research Program, the Deutsche Forschungsgemeinschaft (DFG, German Research Foundation) under Germany's Excellence Strategy – EXC-2094–390783311 (ORIGINS), Project-ID 279384907 - SFB1245, the BMBF via Projects No. 05P15RDFN1, No. EXC-2094-390783311 and the Romanian Ministry of Education and Research through

Contract No. PN 19 06 01 01/2019-2022. Computing resources were provided by the NSCL, the HOKUSAI-Great Wave system at RIKEN, and the Institute for Cyber-Enabled Research at Michigan State University.

*Corresponding author.
esteejus@mit.edu
†Corresponding author.
lynch@frib.msu.edu
‡Corresponding author.
tsang@frib.msu.edu
§Corresponding author.
isobe@riken.jp
‖Corresponding author.
murakami.tetsuya.3e@kyoto-u.ac.jp
¶Corresponding author.
dan.cozma@theory.nipne.ro

[1] B. P. Abbott *et al.* (LIGO Scientific and Virgo Collaborations), GW170817: Observation of Gravitational Waves from a Binary Neutron Star Inspiral, Phys. Rev. Lett. **119**, 161101 (2017).
[2] B. P. Abbott *et al.* (LIGO Scientific and Virgo Collaborations), GW170817: Measurements of Neutron Star Radii and Equation of State, Phys. Rev. Lett. **121**, 161101 (2018).
[3] M. Tsang, W. Lynch, P. Danielewicz, and C. Tsang, Symmetry energy constraints from GW170817 and laboratory experiments, Phys. Lett. B **795**, 533 (2019).
[4] C. Tsang, M. Tsang, P. Danielewicz, W. Lynch, and F. Fattoyev, Insights on Skyrme parameters from GW170817, Phys. Lett. B **796**, 1 (2019).
[5] Y. Lim and J. W. Holt, Neutron Star Tidal Deformabilities Constrained by Nuclear Theory and Experiment, Phys. Rev. Lett. **121**, 062701 (2018).
[6] I. Tews, J. Margueron, and S. Reddy, Critical examination of constraints on the equation of state of dense matter obtained from GW170817, Phys. Rev. C **98**, 045804 (2018).
[7] J. Lattimer and M. Prakash, Neutron star structure and the equation of state, Astrophys. J. **550**, 426 (2001).
[8] A. Drago, A. Lavagno, G. Pagliara, and D. Pigato, Early appearance of Δ isobars in neutron stars, Phys. Rev. C **90**, 065809 (2014).
[9] C. Ducoin, J. Margueron, C. Providência, and I. Vidaña, Core-crust transition in neutron stars: Predictivity of density developments, Phys. Rev. C **83**, 045810 (2011).
[10] J. M. Lattimer and M. Prakash, The equation of state of hot, dense matter and neutron stars, Phys. Rep. **621**, 127 (2016).
[11] J. J. Li and A. Sedrakian, Implications from GW170817 for Δ-isobar admixed hypernuclear compact stars, Astrophys. J. Lett. **874**, L22 (2019).
[12] B. Fore and S. Reddy, Pions in hot dense matter and their astrophysical implications, Phys. Rev. C **101**, 035809 (2020).
[13] P. Danielewicz, R. Lacey, and W. G. Lynch, Determination of the equation of state of dense matter, Science **298**, 1592 (2002).
[14] W. Lynch, M. Tsang, Y. Zhang, P. Danielewicz, M. Famiano, Z. Li, and A. Steiner, Probing the symmetry energy with heavy ions, Prog. Part. Nucl. Phys. **62**, 427 (2009).
[15] A. Le Fèvre, Y. Leifels, W. Reisdorf, J. Aichelin, and C. Hartnack, Constraining the nuclear matter equation of state around twice saturation density, Nucl. Phys. **A945**, 112 (2016).
[16] C. Horowitz, E. Brown, Y. Kim, W. Lynch, R. Michaels, A. Ono, J. Piekarewicz, M. Tsang, and H. Wolter, A way forward in the study of the symmetry energy: Experiment, theory, and observation, J. Phys. G **41**, 093001 (2014).
[17] M. B. Tsang, J. R. Stone, F. Camera, P. Danielewicz, S. Gandolfi, K. Hebeler, C. J. Horowitz, J. Lee, W. G. Lynch, Z. Kohley, R. Lemmon, P. Möller, T. Murakami, S. Riordan, X. Roca-Maza, F. Sammarruca, A. W. Steiner, I. Vidaña, and S. J. Yennello, Constraints on the symmetry energy and neutron skins from experiments and theory, Phys. Rev. C **86**, 015803 (2012).
[18] B.-A. Li, L.-W. Chen, and C. M. Ko, Recent progress and new challenges in isospin physics with heavy-ion reactions, Phys. Rep. **464**, 113 (2008).
[19] W. G. Lynch and M. B. Tsang, The nuclear symmetry energy at sub-saturation densities, arXiv:1805.10757.
[20] N. Ikeno, A. Ono, Y. Nara, and A. Ohnishi, Probing neutron-proton dynamics by pions, Phys. Rev. C **93**, 044612 (2016); Erratum, Phys. Rev. C **97**, 069902 (2018).
[21] M. D. Cozma, Feasibility of constraining the curvature parameter of the symmetry energy using elliptic flow data, Eur. Phys. J. A **54**, 40 (2018).
[22] B.-A. Li, Probing the High Density Behavior of Nuclear Symmetry Energy with High-Energy Heavy Ion Collisions, Phys. Rev. Lett. **88**, 192701 (2002).
[23] B.-A. Li, G.-C. Yong, and W. Zuo, Near-threshold pion production with radioactive beams at the rare isotope accelerator, Phys. Rev. C **71**, 014608 (2005).
[24] J. Hong and P. Danielewicz, Subthreshold pion production within a transport description of central Au + Au collisions, Phys. Rev. C **90**, 024605 (2014).
[25] M. B. Tsang, J. Estee, H. Setiawan, W. G. Lynch, J. Barney, M. B. Chen, G. Cerizza, P. Danielewicz, J. Hong, P. Morfouace, R. Shane, S. Tangwancharoen, K. Zhu, T. Isobe, M. Kurata-Nishimura, J. Lukasik, T. Murakami, and Z. Chajecki (SπRIT Collaboration), Pion production in rare-isotope collisions, Phys. Rev. C **95**, 044614 (2017).
[26] Z. Xiao, B.-A. Li, L.-W. Chen, G.-C. Yong, and M. Zhang, Circumstantial Evidence for a Soft Nuclear Symmetry Energy at Suprasaturation Densities, Phys. Rev. Lett. **102**, 062502 (2009).
[27] M. D. Cozma, The impact of energy conservation in transport models on the π^-/π^+ multiplicity ratio in heavy-ion collisions and the symmetry energy, Phys. Lett. B **753**, 166 (2016).
[28] M. D. Cozma and M. B. Tsang, In-medium $\delta(1232)$ potential, pion production in heavy-ion collisions and the symmetry energy, arXiv:2101.08679.
[29] Y. Blumenfeld, T. Nilsson, and P. Van Duppen, Facilities and methods for radioactive ion beam production, Phys. Scr. **T152**, 014023 (2013).
[30] H. Otsu, S. Koyama, N. Chiga, T. Isobe, T. Kobayashi, Y. Kondo, M. Kurokawa, W. Lynch, T. Motobayashi, T. Murakami, T. Nakamura, M. Kurata-Nishimura, V. Panin, H. Sato, Y. Shimizu, H. Sakurai, M. Tsang, K. Yoneda, and

H. Wang, SAMURAI in its operation phase for RIBF users, Nucl. Instrum. Methods Phys. Res., Sect. B **376**, 175 (2016).

[31] R. Shane *et al.*, SπRIT: A time-projection chamber for symmetry-energy studies, Nucl. Instrum. Methods Phys. Res., Sect. A **784**, 513 (2015).

[32] S. Tangwancharoen, W. G. Lynch, J. Barney, J. Estee, R. Shane, M. B. Tsang, Y. Zhang, T. Isobe, M. Kurata-Nishimura, T. Murakami, Z. Xiao, Y. F. Zhang (SπRIT Collaboration), A gating grid driver for time-projection chambers, Nucl. Instrum. Methods Phys. Res., Sect. A **853**, 44 (2017).

[33] J. Barney, J. Estee, W. G. Lynch, T. Isobe, G. Jhang *et al.*, The sπrit time projection chamber, arXiv:2005.10806.

[34] P. Lasko *et al.*, KATANA—A charge-sensitive triggering system for the SπRIT experiment, Nucl. Instrum. Methods Phys. Res., Sect. A **856**, 92 (2017).

[35] T. Isobe, G. Jhang, H. Baba, J. Barney, P. Baron, G. Cerizza, J. Estee, M. Kaneko, M. Kurata-Nishimura, J. Lee, W. Lynch, T. Murakami, N. Nakatsuka, E. Pollacco, W. Powell, H. Sakurai, C. Santamaria, D. Suzuki, S. Tangwancharoen, and M. Tsang, Application of the generic electronics for time projection chamber (GET) readout system for heavy radioactive isotope collision experiments, Nucl. Instrum. Methods Phys. Res., Sect. A **899**, 43 (2018).

[36] J. Lee, G. Jhang, G. Cerizza, J. Barney, J. Estee, T. Isobe, M. Kaneko, M. Kurata-Nishimura, W. Lynch, T. Murakami, C. Tsang, M. Tsang, R. Wang, B. Hong, A. McIntosh, H. Sakurai, C. Santamaria, R. Shane, S. Tangwancharoen, S. Yennello, and Y. Zhang, Charged particle track reconstruction with SπRIT time projection chamber, Nucl. Instrum. Methods Phys. Res., Sect. A **965**, 163840 (2020).

[37] SπRITROOT Software, https://github.com/SpiRIT-Collaboration/SpiRITROOT/tree/33821f0, accessed January, 9, 2020.

[38] J. Estee, W. Lynch, J. Barney, G. Cerizza, G. Jhang *et al.*, Extending the dynamic range of electronics in a time projection chamber, Nucl. Instrum. Methods Phys. Res., Sect A **944**, 162509 (2019).

[39] C. Tsang, J. Estee, R. Wang, J. Barney, G. Jhang, W. Lynch, Z. Zhang, G. Cerizza, T. Isobe, M. Kaneko, M. Kurata-Nishimura, J. Lee, T. Murakami, and M. Tsang, Space charge effects in the SπRIT time projection chamber, Nucl. Instrum. Methods Phys. Res., Sect. A **959**, 163477 (2020).

[40] J. Barney, Charged pion emission from $^{112}\mathrm{Sn} + {}^{124}\mathrm{Sn}$ and $^{124}\mathrm{Sn} + {}^{112}\mathrm{Sn}$ reactions with the SπRIT time projection chamber, Ph.D. thesis, Michigan State University, 2019.

[41] J. Estee, Charged pion emission from neutron-rich heavy ion collisions for studies on the symmetry energy, Ph.D. thesis, Michigan State University, 2020.

[42] G. Jhang *et al.*, Symmetry energy investigation with pion production from Sn + Sn systems, Phys. Lett. B **813**, 136016 (2021).

[43] M. D. Cozma, Constraining the density dependence of the symmetry energy using the multiplicity and average p_T ratios of charged pions, Phys. Rev. C **95**, 014601 (2017).

[44] G. Ferini, T. Gaitanos, M. Colonna, M. Di Toro, and H. H. Wolter, Isospin Effects on Subthreshold Kaon Production at Intermediate Energies, Phys. Rev. Lett. **97**, 202301 (2006).

[45] T. Song and C. M. Ko, Modifications of the pion-production threshold in the nuclear medium in heavy ion collisions and the nuclear symmetry energy, Phys. Rev. C **91**, 014901 (2015).

[46] S. Huber and J. Aichelin, Production of delta and $N*$ resonances in the one boson exchange model, Nucl. Phys. **A573**, 587 (1994).

[47] A. Larionov and U. Mosel, The $NN \to N\Delta$ cross-section in nuclear matter, Nucl. Phys. **A728**, 135 (2003).

[48] W. Reisdorf *et al.* (FOPI Collaboration), Systematics of central heavy ion collisions in the 1A GeV regime, Nucl. Phys. **A848**, 366 (2010).

[49] W. Reisdorf *et al.* (FOPI Collaboration), Systematics of azimuthal asymmetries in heavy ion collisions in the 1 A GeV regime, Nucl. Phys. **A876**, 1 (2012).

[50] Q. Li, C. Shen, C. Guo, Y. Wang, Z. Li, J. Łukasik, and W. Trautmann, Nonequilibrium dynamics in heavy-ion collisions at low energies available at the GSI Schwerionen synchrotron, Phys. Rev. C **83**, 044617 (2011).

[51] C. J. Batty, S. F. Biagi, E. Friedman, S. D. Hoath, J. D. Davies, G. J. Pyle, and G. T. A. Squier, Shifts and Widths of $2p$ Levels in Pionic Atoms, Phys. Rev. Lett. **40**, 931 (1978).

[52] C. B. Das, S. D. Gupta, C. Gale, and B.-A. Li, Momentum dependence of symmetry potential in asymmetric nuclear matter for transport model calculations, Phys. Rev. C **67**, 034611 (2003).

[53] B. A. Brown, Constraints on the Skyrme Equations of State from Properties of Doubly Magic Nuclei, Phys. Rev. Lett. **111**, 232502 (2013).

[54] Z. Zhang and L.-W. Chen, Constraining the symmetry energy at subsaturation densities using isotope binding energy difference and neutron skin thickness, Phys. Lett. B **726**, 234 (2013).

[55] A. Ono *et al.*, Comparison of heavy-ion transport simulations: Collision integral with pions and Δ resonances in a box, Phys. Rev. C **100**, 044617 (2019).

[56] B. T. Reed, F. J. Fattoyev, C. J. Horowitz, and J. Piekarewicz, Implications of PREX-II on the equation of state of neutron-rich matter, arXiv:2101.03193.

[57] D. Adhikari *et al.*, An accurate determination of the neutron skin thickness of ^{208}Pb through parity-violation in electron scattering, arXiv:2102.10767.

[58] P. Danielewicz, P. Singh, and J. Lee, Symmetry energy III: Isovector skins, Nucl. Phys. **A958**, 147 (2017).

[59] T.-G. Yue, L.-W. Chen, Z. Zhang, and Y. Zhou, Constraints on the symmetry energy from PREX-II in the Multimessenger Era, arXiv:2102.05267.

[60] R. Essick, I. Tews, P. Landry, and A. Schwenk, Astrophysical constraints on the symmetry energy and the neutron skin of ^{208}Pb with minimal modeling assumptions, arXiv:2102.10074.

[61] T. E. Riley, A. L. Watts, S. Bogdanov, P. S. Ray, R. M. Ludlam, S. Guillot, Z. Arzoumanian, C. L. Baker, A. V. Bilous, D. Chakrabarty, K. C. Gendreau, A. K. Harding, W. C. G. Ho, J. M. Lattimer, S. M. Morsink, and T. E. Strohmayer, A NICER view of PSR J0030 + 0451:

Millisecond pulsar parameter estimation, Astrophys. J. **887**, L21 (2019).

[62] M. C. Miller, F. K. Lamb, A. J. Dittmann, S. Bogdanov, Z. Arzoumanian, K. C. Gendreau, S. Guillot, A. K. Harding, W. C. G. Ho, J. M. Lattimer, R. M. Ludlam, S. Mahmoodifar, S. M. Morsink, P. S. Ray, T. E. Strohmayer, K. S. Wood, T. Enoto, R. Foster, T. Okajima, G. Prigozhin, and Y. Soong, PSR J0030 + 0451 mass and radius from NICER data and implications for the properties of neutron star matter, Astrophys. J. **887**, L24 (2019).